Progress In Electromagnetics Research, Vol. 113, 395–412, 2011

SAR IMAGING SIMULATION FOR COMPOSITE MODEL OF SHIP ON DYNAMIC OCEAN SCENE

M. Zhang, Y.-W. Zhao, H. Chen, and W.-Q. Jiang

School of Science
Xidian University, Xi'an 710071, China

Abstract—An efficient double superimposition model (DSM) is proposed to generate two-dimensional (2-D) ocean surface waves. On the basis of this efficient model, a modulated slope-deterministic facet model (MSDFM) is developed to compute the radar cross section (RCS) of synthetic aperture radar (SAR) for the generated ocean surface. Then, the properties of the SAR imaging mechanism for wind seas are discussed from a combination of SAR and ocean wave parameters. Furthermore, a hybrid facet scheme, which is the combination of physical theory of diffraction equivalent edge currents (PTDEEC) and physical optics (PO) method, is introduced to analyze the high frequency scattering characteristics of large ship target. Finally, this hybrid facet scheme combines with the four-path model and MSDFM to investigate SAR imaging for the composite model of ship on dynamic ocean scene. The resolution degradation of ship-ocean model arising from different facet velocities within a SAR resolution cell and the range migration caused by coupling scattering are investigated in this paper. SAR imagery simulations of marine scene are illustrated, proving the validity and practicability of the presented algorithms.

1. INTRODUCTION

SAR images are widely used in many applications, independent of weather condition and sun illumination [1–3]. However, SAR systems utilize sequential Doppler frequency information and Electromagnetic (EM) echo delay of the backscattered signal to resolve targets with high resolution [4, 5]. This makes the SAR sensitive to time-dependent processes such as target motion and multipath effect. So the SAR

Received 11 December 2010, Accepted 1 February 2011, Scheduled 11 February 2011
Corresponding author: Min Zhang (mzhang@mail.xidian.edu.cn).

imaging for the composite model of ship on ocean scene is known to be strongly influenced by the orbital motions of the surface waves and coupling scattering of the ship-ocean model [6–9].

The Doppler shifts induced by the orbital motions of the surface waves distort the phase history of the backscattered signals which are synthesized to get the azimuth resolution. Their effect on the SAR imaging has been studied in many investigations [10–15]. The imaging properties in this regime are studied in detail by these investigations, such as the velocity bunching (VB), velocity smearing parameter, hydrodynamic and tilt cross-section modulation and VB transfer function. However, most theories have been restricted either to the linear mapping regime or to monochromatic ocean waves. Nevertheless, the SAR imaging mechanism of dynamic ocean waves is more complicated, so it is necessary to achieve the accurate mapping computations that can be applied to the realistic case of ocean scene.

A nonlinear imaging spectral calculated from given ocean wave spectra by applying Monte Carlo simulation technique was applied by Alpers to the imaging of one-dimensional (1-D) ocean wave fields [16]. The simulations reveal the basic features of the SAR imaging mechanism, such as the nonlinearity of the imaging, the average velocity bunching parameter suitable for characterizing the degree of nonlinearity, the amount of the azimuth shift of the spectral peak, etc. However, the method was unable to model many important properties of the 2-D mapping process adequately. This includes the most striking characteristic of SAR wave images: the pronounced asymmetries observed between the imaging of range and azimuthally traveling waves. A 2-D Monte-Carlo simulation has been applied in a comparison study of ocean wave spectra measured with a buoy and SAR image spectra obtained over the North Sea during the Shuttle Imaging Radar-B (SIR-B) mission [17]. Besides, a 2-D Monte-Carlo simulation has been made by Bruning et al. to study the nonlinear imaging of a 2-D ocean surface wave field [18]. However, all of the above theories only compute the RCS of SAR by the tilt, hydrodynamic and VB modulation function to the average RCS of the scene. They need some improvement in our opinion.

Likewise, to achieve the SAR image for the composite model of ship on ocean scene, the EM scattering of ship-ocean model should be estimated firstly. There are some high frequency asymptotic methods available for the scattering mechanism of the electrically large object, such as PO method [19], Shooting and Bouncing Rays (SBR) [20, 21] and the method of equivalent edge currents (MEC) [22, 23]. They are flexible and suitable for the calculation of high frequency EM scattering for electric large target. The PO method achieves the

scattering field on the quadrature of the approximate surface induction field. It overcomes the problem of infinity for the plat surface and single curvature surface. However, the contribution of edge diffraction field is not considered in this method. Improved PO models for the evaluation of the field backscattering by triangular trihedral corner reflectors with perfectly conducting faces are developed [24, 25]. They allow a significant improvement to the basic PO model by using the Geometrical Theory of Diffraction (GTD) instead of the Geometrical Optics (GO) to describe the interaction between the corner faces. In fact, besides the lighting by the direct, singly and doubly reflected rays, also that by the rays simply diffracted from the corner edges and by those diffracted and subsequently reflected is taken into account when determining the PO current distribution on each corner face. However these models are virtually unusable due to their computational burden as well as the severe memory requirements. In order to overcome the deficiency, a three-dimensional (3-D) graphics, SBR analysis model which is composed of three general modules has been developed. And the method even like SBR is not so efficient to compute the scattering of very large target. Thus, complexities due to large target size and intricate multi-interactions make the simulation much more stubborn. Therefore, further approximate techniques must be developed. MEC is a progressive method for high frequency which does not need to fill matrix. So it overcomes the disadvantages of the conventional numerical algorithms. But it can not correctly reflect the distribution of the scattering facets, so it also needs some improvement.

In this paper, we attempt a more complete investigation of the SAR imaging mechanism for ocean surface waves based on DSM in which the parameter ranges for the linear and nonlinear imaging regimes are systematically explored. A comprehensive semi-deterministic facet model (SDFM), which is derived from the Kirchhoff Approximation (KA) with Bragg components of the extended Bass-Fuks two-scale model (BFTSM) [26], is developed to compute the RCS of ocean surface waves for real aperture radar (RAR). Then, the MSDFM is achieved by the composition of SDFM with the VB modulation function to compute the RCS of ocean surface waves for SAR. With this method, the SAR image of ocean surface waves can be simulated efficiently and accurately. On the other hand, a hybrid scheme, which combines PTDEEC [27] and PO method, is introduced to analyze the high frequency scattering characteristics of electric large ship target. This method has high efficiency and can correctly reflect the distribution of the scattering facets as well. Further, this method in combination with the MSDFM and four-path model [28, 29] is employed to investigate SAR imaging for the composite model of

ship on ocean scene. The resolution degradation of ship-ocean model arising from the different facet velocities within a SAR resolution cell and the range migration of coupling scattering is investigated in detail with the proposed mechanism.

This paper begins with the large scale modeling of the ocean scene in Section 2. Then, Section 3 shows the ship-ocean wave model for SAR imaging. Subsequently, the backscattering calculation of ship on ocean surface is presented in Section 4. Finally, Section 5 demonstrates the simulation results of ocean scene and ship-ocean model to prove the validity and practicability of the presented algorithms.

2. LARGE SCALE MODELING OF THE OCEAN SCENE

Many approaches were developed to describe the EM scattering from oceanic surface. The most classical one is the two scale model (TSM), which simplifies the sea wave as two configurations: Gravity wave configuration and capillary wave configuration. In this case, the surface spectrum is classified by gravity wave spectrum and capillary wave spectrum respectively. The 2-D gravity ocean wave spectrum in this study is modeled by a JONSWAP spectrum $W_g(k)$ with a frequency dependent spreading factor [30],

$$W_g(k,\phi) = \frac{\alpha}{2}k^{-4}\cdot N(p)\cos^{2p}(\phi-\phi_m) \exp\left\{-\frac{5}{4}\left(\frac{k}{k_c}\right)^{-2}+\ln\gamma\exp\left[-\frac{\left(k^{1/2}-k_c^{1/2}\right)^2}{2\sigma_J^2 k_c}\right]\right\} \quad (1)$$

where, k_c the peak wavenumber, γ the peak enhancement factor, ϕ_m the angle between the wave propagation direction and the flight direction. σ_J is a parameter which describes the width of the JONSWAP spectrum, and $N(p)$ is the spreading function normalization factor.

$$N(p)=\frac{1}{\sqrt{\pi}}\frac{\Gamma(1+p/2)}{\Gamma(1/2+p/2)}, \quad p=\begin{cases}0.46\,(k/k_c)^{2.5}\,p_m & \text{if } k<k_c\\ 0.46\,(k/k_c)^{-1.25}\,p_m & \text{if } k\geq k_c\end{cases} \quad (2)$$

where, $p_m = 11.5\,(U/c_m)^{-2.5}$, U denotes the wind speed at a height of 19.5 m and $c_m = (g/k_c)^{1/2}$ is the phase velocity of the peak wavenumber.

Values of the wave height spectrum, or surface elevation spectral density, are assumed to be specified on a regular grid of spatial wave

numbers:

$$\begin{aligned} k_m &= \frac{2\pi}{L_x}(m - M/2), \quad n = 1, 2 \ldots, N-1 \\ k_n &= \frac{2\pi}{L_y}(n - N/2), \quad m = 1, 2 \ldots, M-1 \end{aligned} \tag{3}$$

where L_x and L_y are the dimensions of the scene in the along-track and across-track directions, respectively. Then (k, ϕ) is the polar coordinates of (k_m, k_n). The large scale structure describes the ocean wave fluctuating on a fixed point by many cosine wave superimpositions. Thus, the surface elevation at time t, for a given realization of the spectrum, may be written as

$$z(x_0, y_0, t) = \sum_{m=1}^{M-1} \sum_{n=1}^{N-1} a_{mn} \cdot \cos(k_m x_0 + k_n y_0 - \omega_{mn} t + \phi_{mn}) \tag{4}$$

where phases ϕ_{mn} are randomly selected from a uniform distribution over $(0, 2\pi)$. Amplitudes a_{mn} are proportional to the square root of gravity ocean wave spectrum, $\omega_{mn} = \sqrt{g(k_m^2 + k_n^2)}$, and g is the gravitational acceleration. Then the orbital velocity and acceleration in range direction are described as the sum of each orbital velocity components.

$$\begin{aligned} & u_r(x_0, y_0, t) \\ &= \sum_{m=1}^{M-1} \sum_{n=1}^{N-1} a_{mn} \omega_{mn} g_{mn} \cdot \cos(k_m x_0 + k_n y_0 - \omega_{mn} t + \phi_{mn} + \phi_v) \end{aligned} \tag{5}$$

$$\begin{aligned} & a_r(x_0, y_0, t) \\ &= -\sum_{m=1}^{M-1} \sum_{n=1}^{N-1} a_{mn} \omega_{mn}^2 g_{mn} \sin(k_m x_0 + k_n y_0 - \omega_{mn} t + \phi_{mn} + \phi_v) \end{aligned} \tag{6}$$

where,

$$g_{mn} = \sqrt{(k_n/k)^2 \sin^2\theta + \cos^2\theta}, \quad \phi_v = \tan^{-1}\left(\frac{k\cos\theta}{k_n \sin\theta}\right) \tag{7}$$

and θ is the incidence angle. Assuming that scatterers are uniformly distributed over the water surface, the average radial velocity over each grid cell of dimensions Δx, Δy and over the integration time T is given by (3) with a_{mn} replaced by $a_{mn} b_{mn}$ [31], here

$$b_{mn} = \sin c\left(\frac{k_m \Delta x}{2}\right) \cdot \sin c\left(\frac{k_n \Delta y}{2}\right) \cdot \sin c\left(\frac{\omega_{mn} T}{2}\right). \tag{8}$$

The radial velocity variance is calculated as the sum of the contributions from each resolved wave component.

3. THE SHIP-OCEAN WAVE MODEL FOR SAR IMGING

The SAR imaging models of ocean wave and ship on ocean surface are achieved in this section.

3.1. The Ocean Wave SAR Imaging Model

If $\omega_{mn}T/2 \leq 1$ and the affection of speckle and system noise to the SAR resolution is neglected. Furthermore, we assume that the scattering at the ocean surface can be described as an aggregate of scattering facets which are statistically independent and the Range-azimuth coupling can be neglected in SAR procession. The SAR imaging model used in this investigation can be based on the generalized velocity bunching model. The Geometric relation between SAR and ocean waves is shown in Fig. 1. After image focused process, the ensemble averaged image intensity $I(x,y)$ of the ocean waves can be expressed by the following integral,

$$\begin{aligned} I^{sea}(x,y) \;=\; & B\int_{-L_x/2}^{L_x/2}\int_{-L_y/2}^{L_y/2} dx_0 dy_0 \sigma_{sea}(x_0,y_0)\cdot \rho_{aN}\big/\rho'_{aN}(x_0,y_0) \\ & \exp\left\{-\pi^{2\cdot}\Big/\rho'_{aN}(x_0,y_0)^2\ [x-x_0-R\cdot u_r(x_0,y_0)/V]^2\right\} \\ & f_y(y-y_0) \end{aligned} \tag{9}$$

here $\sigma_{sea}(x_0,y_0)$ denotes the RCS of ocean that varies along the long ocean wave profile due to tilt, hydrodynamic and velocity bunching, $f_y(\cdot)$ the range resolution function, ρ'_{aN} the degraded azimuth resolution due to target acceleration and finite scene coherence time, R the distance between the target and the radar in range direction and V the platform velocity. B is a constant which depends

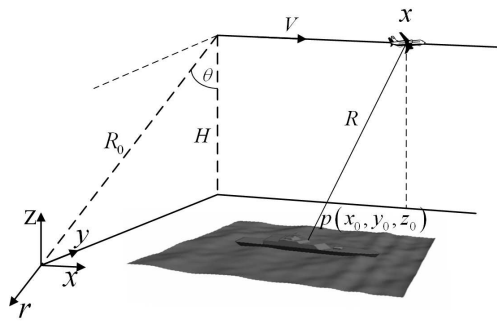

Figure 1. Geometric relation between SAR and marine scene.

on the parameters of the SAR system. The value of B is irrelevant for the present analysis since we are interested in relative changes of $I(x, y)$. The degraded azimuth resolution ρ'_{aN} is given by

$$\rho'_{aN}(x_0, y_0) = \rho_{aN}\left\{1 + \frac{1}{N_l^2}\left[\left(\frac{\pi T^2}{\lambda}a_r(x_0, y_0)\right)^2 + \left(\frac{T}{\tau_s}\right)^2\right]\right\}^{1/2} \quad (10)$$

where, $\rho_a = \lambda R/2TV$ the maximum achievable resolution for one-look and full-bandwidth, $\rho_{aN} = N_l\rho_a$ the stationary target azimuth resolution for N_l incoherent looks, λ the radar wavelength, τ_s the scene coherence time.

3.2. The Ship on Ocean Surface SAR Imaging Model

The geometric relation between SAR and the composite model of ship on ocean scene also obeys Fig. 1. Great efforts have been devoted to tackle the interaction between the ship-like target and ocean surface [29, 32]. The four-path model is a practical method which was firstly released by Johnson [28]. And relative works on the application of this model to marine scene have been released to the estimation of ocean surface influence on radar reflectivity of ships [33], which has been generally regarded as an efficient scheme for the computation of the multiple scattering between the ship and ocean surface. The interactive paths are involved equivalently from the ship target on the basis of the quasi-image method. We consider the SAR imaging model of ship on ocean surface based on this model.

There are some migrations in range for the multi scattering, such as radar-ocean-ship-radar path (path-2), radar-ship-ocean-radar path (path-3) and radar-ocean-ship-ocean-radar path (path-4), since the coupling scattering. The migrations for path-2 and path-3 can be expressed as:

$$\Delta L_2 = \Delta L_3 = \left[4z(x_0, y_0)^2 + R^2 + 4z(x_0, y_0)R\cos\theta\right]^{\frac{1}{2}} - R. \quad (11)$$

And the migrations for path-4 can be expressed as $\Delta L_4 = 2\Delta L_2$. With the help of the complex reflection coefficient ρ fully discussed by [33], we could readily represent the ensemble averaged image intensity $I^{con}(x, r)$ of the ship-ocean model by the following under the four-path diagram:

$$\begin{aligned} I^{con}(x, r) \;=\; & B\left\{\sum I^{dir}(x, r) f_r(r - r_0)\right. \\ & +2|\rho|\sum I^{dir}(x, r) f_r(r - r_0 - \Delta L_2 + \phi_\rho) \\ & \left.+|\rho|^2\sum I^{dir}(x, r) f_r(r - r_0 - \Delta L_4 + 2\phi_\rho)\right\} \quad (12) \end{aligned}$$

with,

$$I^{dir}(x,r) = \sigma_{ship}(x_0,r_0)\exp\left\{-\pi^2\Big/\rho_{aN}(x_0,r_0)^2\ [x-x_0]^2\right\} \quad (13)$$

where, $r_0 = -y_0\sin\theta - z_0\cos\theta$, ϕ_ρ is the phase of the complex coefficient ρ, $\sigma_{ship}(x_0,r_0)$ is the RCS of ship facets.

4. BACKSCATTERING CALCULATION OF SHIP ON OCEAN SURFACE

4.1. Backscattering Calculation of Ocean Surface

In this context, the backscattering calculation of ocean surface is based on the facet approach, which begins with the original formula of Bass and Fuks' composite model. The gravity ocean waves amount to a piecewise planar approximation, shown in Fig. 2. The facet must be large in comparison with the incident wavelength, and be sufficiently small in comparison with the resolution. Note further that each facet must be small enough to correctly approximate the surface height profile. We can get the return of each facet:

$$\langle E_s E_s^* \rangle = 8k_0^4\delta^2 \left\langle F_{p0p}F_{p0p}^* \right\rangle W(q_\perp,\phi)\,\nu(\theta) \quad (14)$$

where δ^2 is the height variance of the small scales at resonant scattering wave number, k_0 the incident wave number, $q_\perp$ the projection of the vector $\vec{q}$ ($\vec{q} = -2\vec{k}_0$) on to the plane tangent, and it is given by $q_\perp = |\vec{q} - \hat{n}\cdot\vec{q}|$. $\hat{n}$ points in the normal direction to the surface facet, that is, $\hat{n} = -z_x\hat{x} - z_y\hat{y} + \hat{z}\Big/\sqrt{1+z_x^2+z_y^2}$, z_x, z_y are the slopes of each facet. The function F_{pop} depends on the incident angle, different for the two polarizations, as well as the local normal unit of each facet. $\nu(\theta)$ is employed to evaluate the shadowing effect, which is discussed by works [34, 35] in detail. $W(k_x,k_y)$ is the 2-D normalized ocean wave

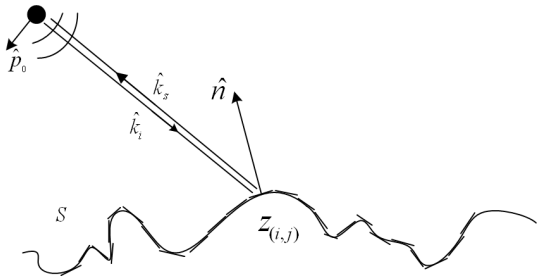

Figure 2. Geometry of a facet scattering surface.

spectrum density, which is expressed in term of the capillary spectrum by $\delta^2 W(k,\phi) = W_c(k,\phi)/k$. Then, Eq. (14) can be rewritten by

$$\langle E_s E_s^* \rangle = 8k_0^4 \nu(\theta) \left\langle F_{p_0 p} F_{p_0 p}^* \right\rangle W_c(k_l, \phi)/k_l \tag{15}$$

where k_l ($k_l = q_\perp$) is the water wave number for resonant scattering; $W_c(k,\phi)$ is the Pierson's capillary spectrum given by Fung and Lee [36] and is expressed by

$$W_c(k,\phi) = 0.875 \cdot (2\pi)^{q-1} \cdot \left(1 + 3k^2/k_c^2\right) g^{(1-q)/2} \times \left[k\left(1+k^2/k_c^2\right)\right]^{-(q+1)/2} \times \left[a_0 + a_1\left(1 - e^{-bk^2}\right)\cos 2\phi\right] \tag{16}$$

Detail information for each parameter above could be found in Ref. [36]. Therefore, from Eq. (15), it could be concluded that, the returns from different facets are proportional to the instantaneous Bragg Fourier components of the capillary spectrum, which leads to statistically independence.

It has clear physical grounds to revise the TSM by a combination of KA with TSM contributions, so called semi-deterministic approach [37]. And the semi-deterministic approach is used in the local summation frame with proper size facets, so we named it semi-deterministic facet model (SDFM). And the return from each facet can be expressed by combing the contributions of the extended BFTSM and the KA solution,

$$\sigma_{SDFM} = \nu(\theta) \left[\sigma_{ij}^{TSM} + \sigma_{ij}^{KA}\right] \Big|_{Z_{xij} \in [\alpha_{ij}] | \alpha_{ij} > -\cot\theta}^{Z_{yij} \in [\beta_{ij}]} \tag{17}$$

$$\sigma_{ij}^{KA} = \pi k^2 q^2 \left| U_{ij}^{p_0 p} \right|^2 \mathbf{Prob}/q_z^4 \tag{18}$$

$$\sigma_{ij}^{TSM} = 8k^4 F_{ij}^{p_0 p} F_{ij}^{p_0 p^*} W_c(K_l, \varphi)/K_l \tag{19}$$

where **Prob** is the Cox-Munk PDF [38]; And $U_{ij}^{p_0 p}$ is polarization-dependent coefficients [39]. The slopes over Z_x have to be limited to $\cot\theta$ to account for the shadowing by large scale waves. In order to filter out the roughness components for which the small perturbation method is inadequate, we ignore the wave number contribution for k_l lower than the cut-off wave number k_d. A strong analysis is made by Hasselmann et al. on the selection of the cutoff wave number [14]. Here, we choose $k_0/4$ empirically. Then the RCS of ocean surface wave facets for RAR from each facet can be basically evaluated by Eq. (17).

When ocean surface waves are imaged by SAR, the scattering elements have varying radial velocities which lead to a spatially varying, nonuniform displacement of the scattering elements in the image plane. As a consequence, the density of the scattering elements in the image plane varies in the flight direction and produces wavelike

patterns in the SAR image. For a relatively small ocean wave parameter range, VB is a linear process. This means that the RCS of ocean surface wave facets for SAR can be calculated in terms of a linear modulation transfer function together with the RCS of ocean surface wave facets for RAR. Thus, the averaged RCS of SAR over Δx, Δy and T are given by

$$\sigma_{sea}(x_0, y_0, t) = \sigma_{SDFM}[1 + f(x_0, y_0, t)] \tag{20}$$

with,

$$\begin{aligned} & f(x_0, y_0, t) \\ = & \sum_{m=1}^{M-1} \sum_{n=1}^{N-1} a_{mn} b_{mn} |R_{vb}| \cdot \cos(k_m x_0 + k_m x_0 - \omega_{mn} t + \phi_{mn} + \phi_R) \end{aligned} \tag{21}$$

where R_{vb} and ϕ_R are the modulus and phase, respectively, of the velocity bunching modulation transfer function,

$$R_{vb}(k_m, k_n) = \frac{R_0}{V} \omega_{mn} (\cos\theta - i \sin\theta \sin\phi_m) \cos\phi_m. \tag{22}$$

Numerical validations on the proposed facet model in monostatic case are discussed on the basis of the experiment by SASS-II, who had been measured the averaged experimental data for Ku and C-bands [40]. Fig. 3 shows the comparisons with the measured data for VV and HH polarization at a wind speed of 5 m/s in upwind. While Fig. 4 displays the comparisons at 10 m/s in upwind. One can see that there is good agreement between the theory and the experiment for VV and HH polarization. Notwithstanding, HH polarization is slightly underestimated for large incidence angles. And it is noted that mismatch in absolute values grows with the wind speed.

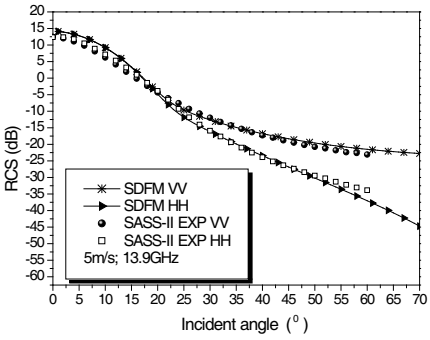

Figure 3. Validation on the impact of polarization mode with wind speed at 5 m/s.

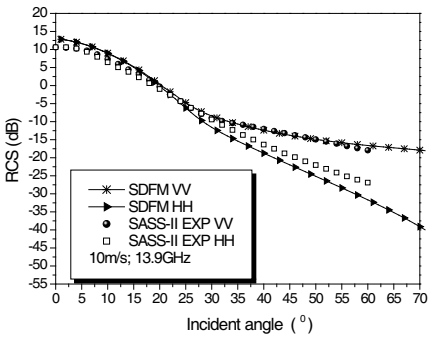

Figure 4. Validation on the impact of polarization mode with wind speed at 10 m/s.

4.2. Backscattering Calculation of Ship Model

The ship-like target is subdivided into triangular facets with the help of CAD tools. A comprehensive method which combines the PO and PTDEEC method is proposed to calculate the EM scattering of ship. PO method is used to compute the facet EM scattering and PTDEEC method is used to compute the edge diffraction. Scattering field of the facet can be calculated by the contour integral of Stratton-Chu [19],

$$E^{PO} = -\frac{2\times\widehat{n}_0\cdot\left(\hat{e}_r\times\hat{h}_i\right)}{w^2}\frac{\exp\left(ik_0R\right)}{4\pi R}\sum_{m=1}^{3}\left(\vec{w}^*\cdot\vec{a}_m\right)\exp\left[\frac{ik_0}{2}\vec{w}\cdot\left(\vec{a}_m+\vec{a}_{m+1}\right)\right]\frac{\sin\frac{1}{2}\left(k_0\vec{a}_m\cdot\vec{w}\right)}{\frac{1}{2}\left(k_0\vec{a}_m\cdot\vec{w}\right)} \tag{23}$$

where $\hat{n}_0$ is the unit normal to the facet; $\hat{e}_r$ is the unit normal to the electric polarization; $\hat{h}_i$ is the unit normal to the magnetic polarization; $\vec{w}$ is the projection of $\left(\hat{k}_i-\hat{k}_s\right)$ onto the facet; $\hat{k}_i$ and $\hat{k}_s$ are the unit vector in the direction of incident wave front and observation point respectively; $\vec{a}_m$ is the n-th edge of the facet and $\vec{a}_m=\vec{a}_{m+1}-\vec{a}_m$.

By using the PTDEEC [27], the scattering fields from the edge of ship-like target is

$$E^{PTDEEC}=-ik\int_c\left[\eta_0 I(\vec{r})\hat{k}_s\times\left(\hat{k}_s\times\hat{t}\right)+M(\vec{r})\left(\hat{k}_s\times\hat{t}\right)\right]\frac{\exp(ikR)}{4\pi R}dl \tag{24}$$

where η_0 is the intrinsic impedance of the medium; $\hat{t}$ is the unit vector along the edge; I and M are the equivalent edge currents assumed at the edge of a planar scattering. The PTDEEC with improved equivalent edge currents by modified edge representation [27] is used in this work. Then, the total scattering field from the ship model is treated as a superimposition of the scattering contributions from PO and PTDEEC method.

$$E^{Total}=E^{PO}+E^{PTDEEC} \tag{25}$$

Therefore, the RCS of the comprehensive ship model is calculated by:

$$\sigma_{ship}\left(x_0,y_0\right)=4\pi\lim_{R_0\to\infty}R_0^2\frac{\left|E^{Total}\right|^2}{\left|E_{inc}\right|^2} \tag{26}$$

The comparison of RCS between the proposed method and MEC is shown in Figs. 5 and 6. The detail parameters are fixed as follows: incident frequency: 10 GHz; incident angle 60°. We can see that the calculated results are in good agreement. But our method is more applicable to SAR imaging simulation.

5. SIMULATION RESULTS OF OCEAN SCENE AND SHIP-OCEAN MODEL

In generating realizations of the SAR images for the ocean surface wave field, the JONSWAP form is used for growing windsea spectra and fully developed spectra with appropriate choice of parameters respectively shown in Table 1. The corresponding sea surface elevation images are shown in Figs. 7(a), 8(a) and 9(a). The SAR parameters used in the simulation work are selected for general spaceborne SAR (SPA-SAR) and airborne SAR (AIR-SAR) respectively in Table 2. And the corresponding SAR images are displayed in Figs. 7(b)–(c), 8(b) and 9(b). It is shown that the azimuth resolution is degraded with the reduction of ϕ_m, increase of R/V and λ. The modulation of velocity

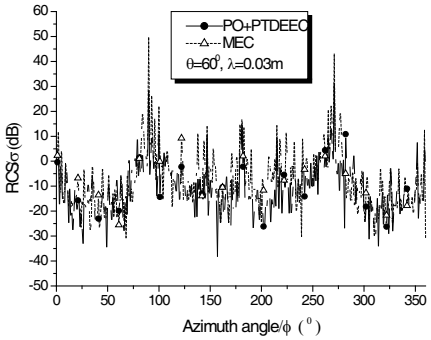

Figure 5. RCS of the ship model at VV polarization.

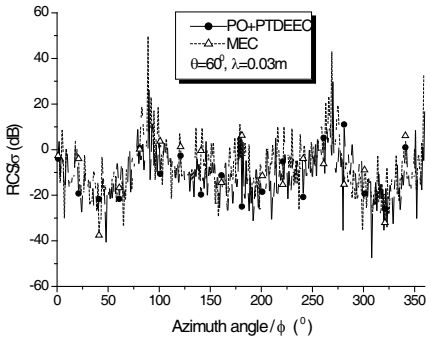

Figure 6. RCS of the ship model at HH polarization.

Table 1. Ocean parameters used in the simulation.

Sea state	α	γ	ϕ_m (°)	U (ms^{-1})
Growing windsea	0.01	3.3	60°	10
Developed I	0.0081	1	60°	10
Developed II	0.0081	1	60°	5

Table 2. SAR parameters used in the simulation.

Parameter / SAR	λ (m)	θ(°)	ρ_a (m)	T (s)	R/V	N_1
SPA-SAR	0.23	25°	6.0 m	2.25 s	120 s	4
AIR-SAR	0.03	60°	4.5 m	0.2 s	60 s	2

bunching is sensitive to the direction of sea wave propagation. Position migration and image blur are more serious with the increase of wind velocity.

The SAR images of the ship on ocean scene model are shown in Figs. 10(a)–(b). The ship body is along-track and across-track respectively. It is demonstrated that the coupling scattering of ship and ocean surface cause the range migration in SAR images, especially for the EM scattering from the side of ship. And the strong scattering sources of the ship-ocean model, such as the corner reflector, antennas and the edge of the board, are evident in the imageries, demonstrating the practicability of the proposed methods.

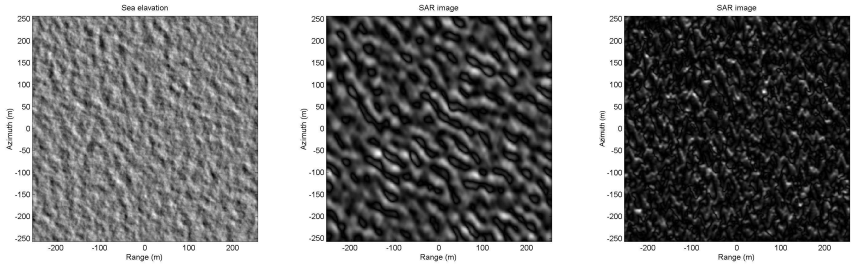

Figure 7. (a) Sea surface elevation (Growing windsea). (b) SPA-SAR image (Growing windsea). (c) AIR-SAR image (Growing windsea).

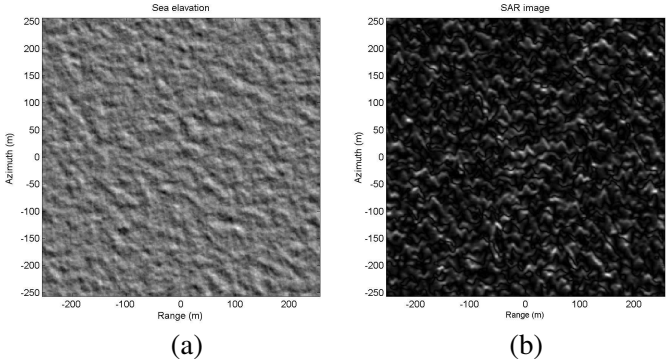

Figure 8. (a) Sea surface elevation (Developed I). (b) AIR-SAR image (Developed I).

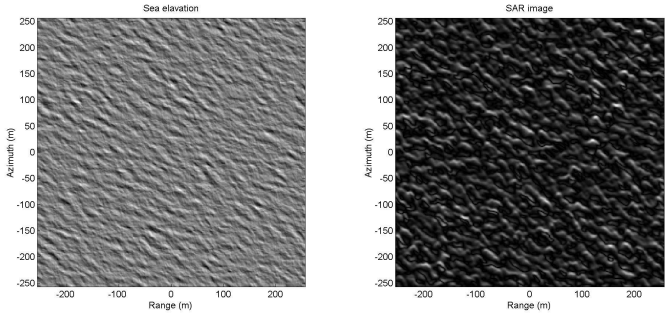

Figure 9. (a) Sea surface elevation (Developed II). (b) AIR-SAR image (Developed II).

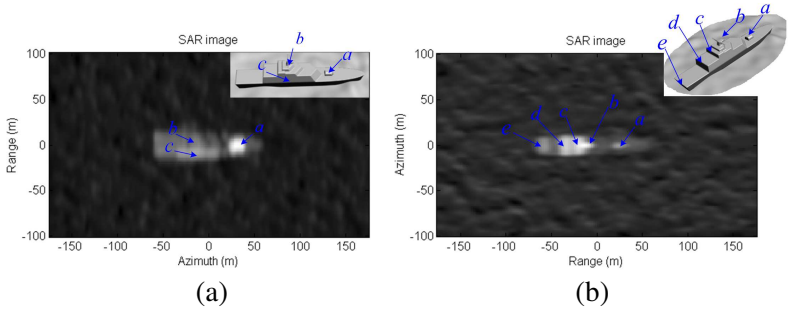

Figure 10. (a) AIR-SAR image of ship-ocean model (Developed II). (b) AIR-SAR image of ship-ocean model (Developed II).

6. CONCLUSION

In this paper, the efficient SAR imaging simulation work of ocean surface and ship on ocean surface model is carried out. The RCS of SAR for the sea surface is computed by the model of MSDFM, which is the SDFM together with transfer function of VB. Furthermore, the high frequency scattering characteristics of ship target is computed by a hybrid facet scheme, which is the combination of PTDEEC and PO method. Finally, this hybrid facet scheme is combined with the four-path model and MSDFM to investigate SAR imaging of a ship on sea surface scene. Then, the properties of the SAR imaging mechanism for windseas and ship on ocean surface model are discussed from a combination of SAR, ocean wave and ship facet parameters. It demonstrates that the resolution degradation of ship-ocean model

arises from the different facet velocities within a SAR resolution cell and the range migration caused by coupling scattering. In addition, the imaging is strongly dependent on the mean ocean wave propagation direction ϕ_m relative to the sensor flight direction. All of these effects have been observed in SAR images.

ACKNOWLEDGMENT

This work was supported in part by the National Natural Science Foundation of China under Grant No. 60871070, the National Pre-research Foundation and the Foundation of the National Electromagnetic Scattering Laboratory to support this kind of research.

REFERENCES

1. Jin, Y.-Q., "Polarimetric scattering modeling and information retrieval of SAR remote sensing — A review of FDU work," *Progress In Electromagnetics Research*, Vol. 104, 333–384, 2010.
2. Teng, H. T., H.-T. Ewe, and S. L. Tan, "Multifractal dimension and its geometrical terrain properties for classification of multi-band multi-polarized SAR image," *Progress In Electromagnetics Research*, Vol. 104, 221–237, 2010.
3. Park, J.-I. and K.-T. Kim, "A comparative study on isar imaging algorithms for radar target identification," *Progress In Electromagnetics Research*, Vol. 108, 155–175, 2010.
4. Chan, Y. K. and V. C. Koo, "An introduction to synthetic aperture radar (SAR)," *Progress In Electromagnetics Research B*, Vol. 2, 27–60, 2008.
5. Mao, X., D.-Y. Zhu, and Z.-D. Zhu, "Signatures of moving target in polar format spotlight SAR image," *Progress In Electromagnetics Research*, Vol. 92, 47–64, 2009.
6. Li, X. M., S. Lehner, and M. X. He, "Ocean wave measurements based on satellite synthetic aperture radar (SAR) and numerical wave model (WAM) data-extreme sea state and cross sea analysis," *International Journal of Remote Sensing,* Vol. 29, 6403–6416, 2008.
7. Margetis, D., "Pulse propagation in sea water: The modulated pulse," *Progress In Electromagnetics Research*, Vol. 26, 89–110, 2000.
8. Zecchetto, S., F. de Biasio, and P. Trivero, "A wavelet technique

to extract the backscatter signatures from SAR images of the sea," *PIERS Online*, Vol. 5, No. 7, 696–700, 2009.

9. Luo, W., M. Zhang, Y. W. Zhao, and H. Chen, "An efficient hybrid high-frequency solution for the composite scattering of the ship on very large two-dimensional sea surface," *Progress In Electromagnetics Research M*, Vol. 8, 79–89, 2009.
10. Valenzuela, G. R., "An asymptotic formulation for SAR images of the dynamical ocean surface," *Radio Science,* Vol. 15, 104–114, 1980.
11. Raney, R. K., "Wave orbital velocity, fade and SAR response to azimuth waves," *Journal of Oceanic Engineering*, Vol. 6, 140–146, 1981.
12. Plant, W. J. and W. C. Keller, "The two-scale radar wave probe and SAR imagery of the ocean," *Journal of Geophysical Research*, Vol. 88, 9776–9784, 1983.
13. Zhao, Y. W., M. Zhang, and H. Chen, "An efficient ocean SAR raw signal simulation by employing fast fourier transform," *Journal of Electromagnetic Waves and Applications* Vol. 24, No. 16, 2273–2284, 2010.
14. Hasselmann, K., R. K. Raney, W. J. Plant, W. Alpers, R. A. Shuchnan, D. R. Lyzenga., C. L. Rufenach, and M. J. Tucker, "Theory of synthetic aperture radar ocean imaging: A marsen view," *Journal of Geophysical Research*, Vol. 90, 4659–4685, 1985.
15. Lim, S.-H., J.-H. Han, S.-Y. Kim, and N.-H. Myung, "Azimuth beam pattern synthesis for airborne SAR system optimization," *Progress In Electromagnetics Research*, Vol. 106, 295–309, 2010.
16. Alers, W., "Monte Carlo simulations for studying thc relationship between ocean wave and synthetic aperture radar image spectra," *Journal of Geophysical Research*, Vol. 88, 1745–1759, 1983.
17. Alpers, W., C. Bruning, and K. Richter, "Comparison of simulated and measured synthetic aperture radar image spectra with buoy-derived ocean wave spectra during the shuttle imaging radar-B mission," *IEEE Trans. Geosci. Remote Sens.*, Vol. 24, 559–566, 1986.
18. Bruning, C., W. Alpers, and K. Hasselmann, "Monte-Carlo simulation studies of the nonlinear imaging of a two dimensional surface wave field by a synthetic aperture radar," *International Journal of Remote Sensing*, Vol. 11, 1695–1727, 1990.
19. Gorden, W. B., "Far-field a pproximations to the Kirchoff-Helmholtz representations of scattered fields," *IEEE Trans.*

Antennas Propagat., Vol. 23, No. 4, 590–592, 1975.

20. Yu, C. L., "Radar cross section computation and visualization by shooting and bounching ray (SBR) technique," *IEEE Trans. Antennas Propagat.*, Vol. 3, 1323–1326, 1992.
21. Kim, B. C., K. K. Park, and H. T. Kim, "Efficient RCS prediction method using angular division algorithm," *Journal of Electromagnetic Waves and Applications*, Vol. 23, No. 1, 65–74, 2009.
22. Michaeli, A., "Equivalent edge currents for arbitrary aspects of observation," *IEEE Trans. Antennas Propagat.*, Vol. 32, 252–258, 1984.
23. Baussard, A., M. Rochdi, and A. Khenchaf, "PO/mec-based scattering model for complex objects on a sea surface," *Progress In Electromagnetics Research*, Vol. 111, 229–251, 2011.
24. Corona, P. and G. Ferrara, "An improved physical optics model for the evaluation of the field backscattering by triangular trihedral corner reflectors," *Electrotechnical Conference*, Vol. 1, 534–537, May 1996.
25. Zhang, P. F. and S. X. Gong, "Improvement on the forwardbackward iterative physical optics algorithm applied to computing the RCS of large open-ended cavities," *Journal of Electromagnetic Waves and Applications*, Vol. 21, No. 4, 457–469, 2007.
26. Chen, H., M. Zhang, and D. Nie, "Robust semi-deterministic facet model for fast estimation on EM scattering from ocean-like surface," *Progress In Electromagnetics Research B*, Vol. 18, 347–363, 2009.
27. Wu, Z. S. and M. Zhang, "Improved equivalent edge currents by modified edge representation and their application in EM scattering," *Acta Electronica Sinica*, Vol. 26, No. 9, Sep. 1998.
28. Johnson, J. T., "A study of the four-path model for scattering from an object above a half space," *Microwave Opt. Technol. Lett.*, Vol. 30, No. 6, 130–134, 2001.
29. Dong, C. Z., C. Wang, X. Wei, and H.-C. Yin, "EM scattering from complex targets above a slightly rough surface," *PIERS Online*, Vol. 3, No. 5, 685–688, 2007.
30. Mitsuyasu, H., F. Tasai, T. Suhara, S. Mizuno, M. Ohkusu, T. Honda, and K. Rikiischi, "Observations of the directional spectrum of ocean wave using a clover leaf buoy," *Journal of Physical Oceanography*, Vol. 5, 750–760, 1975.
31. Lyzenga, D. R., "Numerical simulation of synthetic aperture radar image spectra for ocean waves," *IEEE Trans. Geosci. Remote*

Sens, Vol. 24. 1986.

32. Zhang, Y., Y. E. Yang, H. Braunisch, and J. A. Kong, "Electromagnetic wave interaction of conducting object with rough surface by hubrid SPM/MOM technique," *Progress In Electromagnetics Research*, Vol. 22, 315–335, 1999.
33. Shtager, E. A., "An estimation of sea surface influence on radar reflectivity of ships," *IEEE Trans. Antennas Propagat.*, Vol. 47, No. 10, 1623–1627, 1999.
34. Bourlier, C., G. Berginc, and J. Saillard, "One and two-dimensional stationary shadowing functions for any height and slope stationary uncorrelated surface in the monostatic and bistatic configureations," *IEEE Trans. Antennas Propagat.*, Vol. 50, No. 3, 312–324, 2002.
35. Fabbro, V., C. Bourlier, and P. F. Combes, "Forward propagation modeling above gaussian rough surfaces by the parabolic shadowing effect," *Progress In Electromagnetics Research*, Vol. 58, 243–269, 2006.
36. Fung, A. K. and K. Lee, "A semi-empirical sea-spectrum model for scattering coefficient estimation," *IEEE J. Oceanic Engineering*, Vol. 7, No. 4, 166–176, 1982.
37. Andreas, A. B., A. Khenchaf, and A. Martin, "Bistatic radar imaging of the marine environment. Part I: Theoretical background," *IEEE Trans. Geosci. Remote Sens.*, Vol. 45, No. 11, 3372–3383, 2007.
38. Cox, C. and W. H. Munk, "Statistics of the sea surface derived from sun glitter," *J. Marine Res.*, Vol. 13, 198–227, 1954.
39. Ulaby, F. T., R. K. Moore, and A. K. Fung, *Microwave Remote Sensing*, Addison-Wesley Publishing Company, Canada, 1982.
40. Voronovich, A. G. and V. U. Zavorotni, "Theoretical model for scattering of radar signals in Ku- and C-bands from a rough sea surface with breaking waves," *Wave in Random Media*, Vol. 11, No. 3, 247–269, 2001.